13th World Conference on Earthquake Engineering
Vancouver, B.C., Canada
August 1-6, 2004
Paper No. 2045

OUT-OF-PLANE DYNAMIC RESPONSE OF UNREINFORCED MASONRY BEARING WALLS ATTACHED TO FLEXIBLE DIAPHRAGMS

Can C. SIMSIR[1], Mark A. ASCHHEIM[2] and Daniel P. ABRAMS[3]

SUMMARY

The paper summarizes research on the out-of-plane behavior of unreinforced masonry bearing walls in buildings subjected to earthquake motions. Results from a set of shake table tests revealed that, in general, the walls performed very well despite the intensity of the base motion and the slenderness of the wall. Experimental results are compared with those simulated using SDOF and MDOF computational models. The validated models are useful for establishing that permissible limits on wall slenderness as prescribed by current seismic guidelines (FEMA356) can be increased. A two-degree-of-freedom model is introduced as a simple tool for dynamic stability analysis of unreinforced masonry walls.

INTRODUCTION

Based on observations in past earthquakes, engineers have been concerned that earthquakes can cause the collapse of load bearing masonry walls responding out of plane, especially in buildings having relatively flexible floor diaphragms. This concern is particularly relevant to the central and eastern United States, where unreinforced masonry (URM) buildings are the most common type of structure among essential facilities (French and Olshansky [9]) and nearly always were designed and constructed with no consideration for seismic actions. Residential buildings as well as hospitals, schools, and fire and police stations whose functionality is essential to post-earthquake recovery are mostly URM structures and would suffer heavy damage causing loss of life in the event of a moderate or strong earthquake.

The concern for the existing large URM building population in seismically hazardous regions has prompted several researchers to perform laboratory tests of URM walls responding out of plane. Among these researchers, the ABK Joint Venture performed the most extensive series of dynamic tests on the URM out-of-plane walls in the early 1980s that remain the primary source for today's guidelines for seismic design and evaluation (e.g. FEMA 356 [8]).

[1] Ph.D. Candidate, University of Illinois, Urbana, USA. Email: simsir@uiuc.edu
[2] Associate Professor, Santa Clara University, California, USA. Email: maschheim@scu.edu
[3] Professor, University of Illinois, Urbana, USA. Email: d-abrams@uiuc.edu

The ABK Joint Venture performed tests on reinforced and unreinforced masonry walls loaded dynamically in the out-of-plane direction (ABK [1], [2]). The unreinforced clay brick and concrete block masonry walls had different slenderness ratios (wall height / wall thickness). A constant axial load was applied by means of a weight suspended from the top of the wall. Controlled lateral displacement histories were applied dynamically by separate servo-hydraulic actuators at the top and bottom of each wall. Displacement histories applied at the top of the wall were amplified to simulate the effects of floor diaphragm flexibility. Most of the URM walls cracked horizontally approximately at their mid-heights and near the base well before failure. Collapse occurred as the mid-height cracks opened substantially, leading to instability.

Based on these tests, Kariotis et al. [11] and Adham [3] identified allowable wall slenderness ratios as a function of the overburden ratio (superimposed weight / wall weight) and peak input velocities at the top and base of the wall. Current seismic provisions for the rehabilitation of existing buildings, FEMA 356 [8] provide permissible slenderness ratios for URM walls based on the potential for out-of-plane failure (Table 2). For damaged walls, these ratios are even smaller (FEMA 306 [6]). The tabulated values are based on the work done by ABK [1, 2] in the early 1980s, although they are tabulated as a function of design spectral acceleration rather than in terms of velocities as originally put forth by ABK in Table 1. The tests performed by ABK also serve as the only reference in FEMA 307 [7] for experimental research that addresses the out-of-plane flexural behavior mode of unreinforced masonry walls.

Table 1. ABK slenderness (h/t) values.

WALL TYPES	Buildings with crosswalls	All Other Buildings
Walls of one-story buildings	20	14
First-story wall of multistory building	20	20
Walls in top story of multistory building	14	9
All other walls	20	15

Table 2. FEMA 356 slenderness (h/t) values.

WALL TYPES	S_{x1}* < 0.24g	0.24g < S_{x1} < 0.37g	0.37g < S_{x1} < 0.5g
Walls of one-story buildings	20	16	13
First-story wall of multistory building	20	18	15
Walls in top story of multistory building	14	14	9
All other walls	20	16	13

* S_{x1}: Spectral response acceleration at 1-second period.

In more recent years, several other dynamic tests of URM walls responding out of plane have been performed. A discussion on some of these test setups and results is presented by Simsir et al. [15]. Simsir et al. [14] provides also a summary of past quasi-static tests for out-of-plane response as well as shake table tests of URM parapet walls.

Past test setups have either neglected the influence of floor diaphragm flexibility (by using a rigid steel frame to attach the top and bottom of the out-of-plane walls) or failed to represent realistically the seismic loading on URM out-of-plane walls in buildings with flexible diaphragms.

This paper summarizes research that aims at addressing the influence of floor diaphragm flexibility on wall stability by performing shake table tests on an idealized low-rise URM building model that includes a floor diaphragm as well as in-plane and out-of-plane wall components. Described are the experimental program including the test specimens and test results, and the analytical models including single, multi, and two degree-of-freedom models. Experimental results are compared with those of the response simulations with the analytical models. The mid-height cracking and mid-height failures observed in

previous out-of-plane dynamic tests of URM walls did not develop in these tests; explanations for this difference are offered.

EXPERIMENTAL PROGRAM

Test Specimens

An idealized model that represents essential features of a masonry building was constructed on the earthquake simulator (shake table) of the Newmark Structural Engineering Laboratory at the University of Illinois. Although there was no prototype building for the model, it possessed characteristics of a typical, low-rise URM building. Since the research focuses on the response of bearing walls responding out of plane, these typical building characteristics included the slenderness of the out-of-plane walls, axial stress on the out-of-plane walls, the stiffness of the diaphragm and the period of vibration of the structure.

The major components of the test structure were the floor (or roof) diaphragm as well as two in-plane and two out-of-plane free-standing wall components. The out-of-plane and in-plane walls were transverse and parallel to the direction of shaking, respectively. The out-of-plane walls were bearing walls supporting the gravity load of the floor mass, while the in-plane walls were shear walls since they resisted the inertial forces from the floor mass. The test set-up was built to investigate the response of out-of-plane wall component as an integral part of the building system. This is illustrated in Figure 1; the test structure is shown in Figure 2.

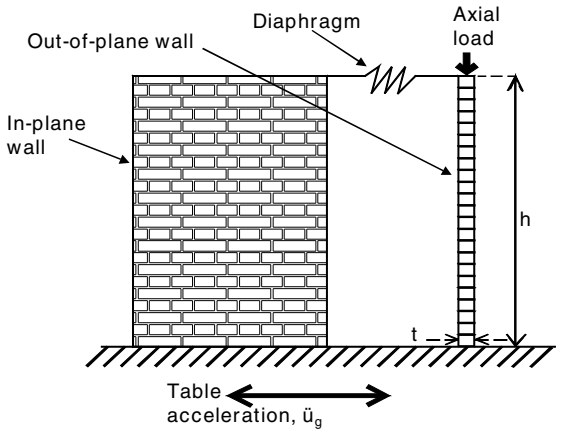

Figure 1. Illustration of the test setup.

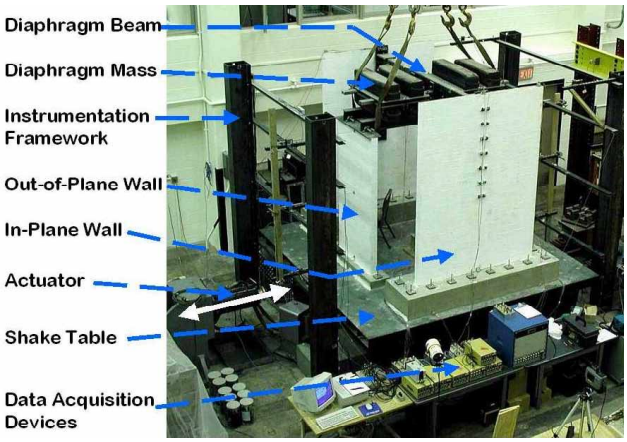

Figure 2. Specimen on the shake table.

All walls were built from half-scale lightweight concrete hollow blocks with each block having dimensions 7⅝ x 3⅝ x 3⅝ inch (194 x 92 x 92 mm), and a density of 96 pcf (1540 kg/m^3).

The out-of-plane walls were URM bearing walls designed to support the gravity load of the floor mass. This load was applied concentrically to the out-of-plane walls to create an axial stress on the net cross-section of the block, representative of the stress in the ground story walls of a three-story building. Low strength, Type O mortar was used for the out-of-plane walls to mimic the weak materials in many existing URM buildings in the United States. The walls were not grouted. Each of the two out-of-plane wall panels had a slenderness (height-to-thickness or h/t) ratio of 21.0, nearly equal to the largest permissible value of 20 allowed in the current seismic guidelines FEMA 356 [8]. This document allows larger slenderness ratios to be used if justified by a dynamic stability analysis, but methods for conducting such an analysis are not specified, making them largely subject to the discretion of the user.

The in-plane walls were adequately reinforced with vertical and horizontal steel reinforcing bars, and were fully grouted. High strength, Type S mortar was used for these walls. The reinforcement assured that the integrity of the in-plane walls would be maintained throughout the experimental program.

A series of material tests were performed to determine the strength properties of the mortar, block, masonry, grout and reinforcement. Results from some of these tests as well as a more detailed description of the masonry walls are presented by Simsir et al. [14].
The lateral stiffness of the diaphragm as well as the floor and out-of-plane wall weights were varied. Table 3 presents specimen definitions identified for varied properties of test specimens. Apart from the floor mass reduction in test specimen S3, the weight of one of the out-of-plane walls (the West Wall) was nearly tripled by bolting lead ingots to both faces of the wall along its height. The ingots were bolted on to the blocks, and not on to the mortar bedjoints in order not to change the wall's out-of-plane stiffness.

Table 3. Specimen number definitions.

Test Specimen	Diaphragm Beam	Floor Mass
S1	Stiff	6.50 kips
S2	Flexible	6.50 kips
S3	Flexible	3.50 kips

The floor mass (see Table 3) was supported on the two out-of-plane walls by means of a pin connection, which allowed rotation at the top of the wall with respect to the diaphragm, while keeping the gravity load applied concentrically on the wall. Simsir et al. [14] provides further information on the connection details between the masonry walls and the diaphragm beam, and between the diaphragm and floor mass.

The test structure included a steel beam to represent the lateral stiffness of a timber floor diaphragm. The beam had to be as flexible as a wood diaphragm, yet strong enough to be able to bear the inertial load without yielding prematurely. Two steel beams, each with a different rectangular hollow cross-section (tube section) were used representing two diaphragms having different stiffnesses. Either tube section spanned 100 inches (2540 mm) in weak-axis bending between pins attached to the two in-plane walls. The lateral stiffnesses of the stiff and flexible tubes were calculated as 32.90 kips/in and 3.71 kips/in, respectively. The stiff tube had 8.87 times the lateral stiffness of the flexible one.

The selection of the stiff tube was dictated by a design objective to achieve a short natural period of vibration (around 0.1 s.) for the test structure such that the period was on the ascending portion of the acceleration response spectrum of the simulated earthquake ground motion. For the flexible tube, a longer period (around 0.4 s.) that was on the descending portion of the acceleration response spectrum was desired. Also, these values compared well with the natural periods in the two horizontal directions (0.15 and 0.40 s.) of a three-story police station in Carbondale, Illinois, based on a finite element model of this typical URM structure created by Wen and Liao [16].

Figure 3 shows a comparison of the force-displacement curves of the two tubes with those of the three diaphragm subassembly specimens tested by Peralta et al. [12]. The three specimens were tested to examine the performance of existing floor and roof diaphragms in the Midwest. The three curves shown in the figure are bilinear approximations of the backbone curves from quasi-static reversed cyclic loading. The two curves for the tubes are assumed elastoplastic considering there is only 10% increase in strength between yield and ultimate as specified by the tube manufacturer.

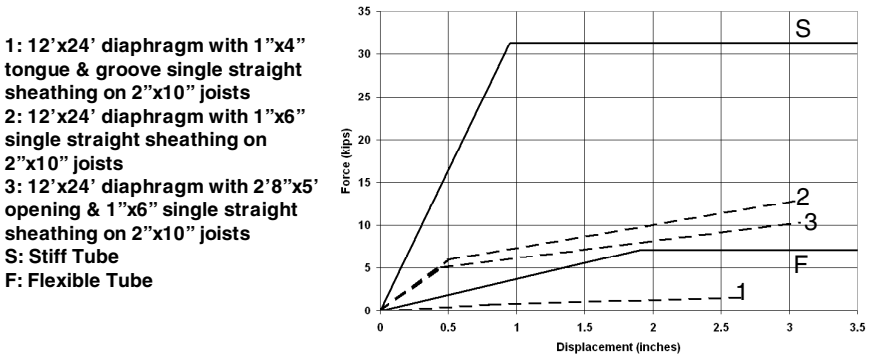

Figure 3. Comparison of steel tubes to wood diaphragms.

Tests

The shake table simulated unidirectional earthquake ground motions to perform dynamic tests of the structure. A total of 22 signals were applied with increasing amplitude to determine the damage level associated with the amplitude. For each run, the specimen type, the name of the ground motion record, the peak table acceleration, the maximum measured displacements and accelerations at the top and mid-height of one of the out-of-plane walls (the East Wall) are given in Table 4. The measured values for the West out-of-plane wall were similar (except for the 22nd run when the West Wall collapsed) to those of the East Wall, and therefore are not listed for brevity. Displacements were relative to the displacements measured at the base of the wall; accelerations were absolute values.

Table 4. Shake table runs and the recorded peak values for the East out-of-plane wall.

Run Number*	Test Specimen	Record Name	Peak Table Acceleration (g)	Displacements (in)		Accelerations (g)	
				Top	Mid-height	Top	Mid-height
1	S1	Nahanni	0.056	0.033	0.017	0.047	0.100
2	S1	Nahanni	0.109	0.064	0.027	0.121	0.113
3	S1	Nahanni	0.150	0.155	0.079	0.518	0.491
4	S1	Nahanni	0.192	0.199	0.097	0.812	0.747
5	S1	Nahanni	0.220	0.225	0.120	1.199	0.811
6	S1	Nahanni	0.267	0.217	0.110	0.974	0.971
7	S1	Nahanni	0.341	0.269	0.137	1.249	1.284
8	S1	Nahanni	0.482	0.298	0.156	1.735	1.803
9	S1	Nahanni	0.650	0.443	0.249	4.132	4.598
10	S1	Nahanni	0.912	0.577	0.329	2.996	3.554
11	S1	Nahanni	0.256	0.132	0.064	0.501	0.481
12	S1	Nahanni	1.167	0.534	0.290	2.766	2.906
13	S1	Big Bear	0.386	0.200	0.106	0.670	0.644
14	S1	Big Bear	0.625	0.353	0.188	1.984	1.526
16	S1	Big Bear	1.203	0.699	0.371	3.142	2.504
17	S2	Big Bear	0.125	0.465	0.233	0.318	0.462
18	S2	Big Bear	0.369	1.263	0.664	0.896	1.221
19	S2	Big Bear	0.618	1.767	0.934	1.130	1.545
20	S2	Big Bear	1.078	2.510	1.331	1.508	1.356
21	S3	Big Bear	0.126	0.548	0.295	0.584	0.653
22	S3	Big Bear	0.365	1.366	1.206	1.728**	2.036**

* Values for the 15th run are not shown due to a recording error that occurred during testing when the shake table reached its displacement limit and the servoram driving the table had to shut off.

** These are peak values for the first 6 seconds of the record after which larger values were measured due to impact of the collapsing West out-of-plane wall on the table platform.

Ground acceleration histories from 1985 Nahanni and 1992 Big Bear earthquakes were used as input excitations to the shake table. Some characteristics of the two earthquakes that were recorded at freefield strong motion stations are given in Table 5. The earthquakes were selected for this study due to several reasons that are described by Simsir et al. [15], which also plots the accelerograms from these ground motions.

Table 5. Characteristics of recorded earthquake ground motions used in the dynamic tests.

Earthquake Name	NAHANNI	BIG BEAR
Location	Northwest Territories, Canada	southern California, USA
Date	23 December 1985	28 June 1992
Magnitude, Ms	6.9	6.6
Depth (km)	6	7
Station	#60907 Battlement Creek Site	#22561 Civic Center Grounds
Station Type	freefield strong motion	freefield strong motion
Site Geology	carbonate and clastic sedimentary rocks at least 8 to 10 km deep underlain by Canadian Shield rock	shallow alluvium over granite bedrock
Epicentral Distance (km)	8	12
Component	010 horizontal	360 horizontal
PGA (g)	1.102	0.545
Duration (s)	20	20

Through the experimental program, several free vibration and series of low amplitude forced vibration tests were performed to monitor the shift in the natural frequency of vibration of the test structures, as shown in Figure 4. The frequencies measured during the free vibration tests were consistently larger than those measured during the frequency sweep tests. Often the natural frequency of vibration decreased after a dynamic test, indicating softening of the specimen due to damage during the test. Considering the frequency sweep test results, the natural frequency of S1 with the stiff diaphragm decreased from an initial value of 6.35 Hz to 4.35 Hz by the end of the 16th dynamic test run. Being a more flexible specimen, S2 had a smaller initial natural frequency of 2.53 Hz that decreased to 2.44 Hz after the 20th run. S3 had a larger initial value of 3.30 Hz considering its significantly decreased floor mass.

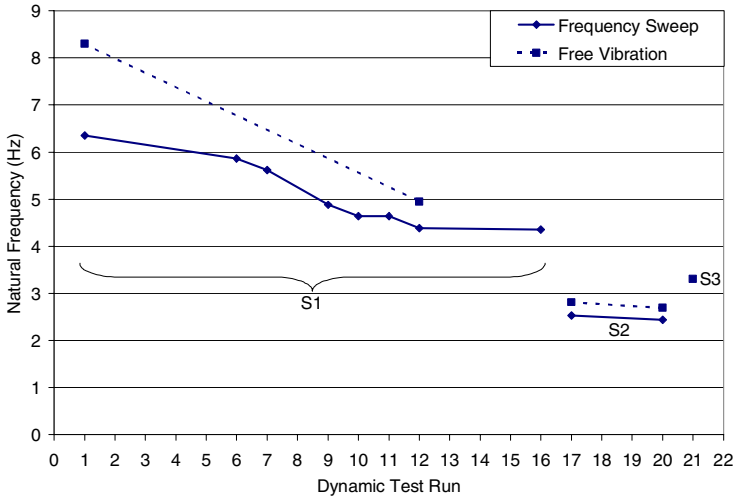

Figure 4. Variation of the natural frequency of the test structures.

Simsir et al. [14, 15] presents the variation of the period of vibration for S1, S2 and S3 specimens over the displacement and pseudo acceleration response spectra for Nahanni and Big Bear motions. Through a response spectrum analysis, spectral displacements were computed at the top of the out-of-plane walls, which correlated well with the measured displacement values (Simsir et al. [14]).

Test Results

Horizontal cracks at the base of the out-of-plane walls were observed for the first time after the 7th test run, and they became more pronounced in subsequent runs 9, 10, and 12. These cracks, identified as crack #1 in Figure 5a, were located at the bedjoint between the bottom course and the concrete footing. No cracks developed above the base of the out-of-plane walls during the first 21 runs. The observed behavior of both walls resembled that of a rigid body rocking about the bedjoint crack #1. The two walls connected to each other by the axially rigid floor mass rocked back and forth in phase. The observed near-rigid-body-rocking behavior was verified by the measured response at the top, mid-height, and base of the walls, discussed in detail by Simsir et al. [14]. The displacements of the out-of-plane walls increased with increasing intensity of ground acceleration (Table 4), with the maximum response obtained during the 20th run in which the walls had a drift ratio of 3.4%. There were no lateral offset or spalling of mortar at the base cracks. The walls did not slide relative to their footings or the shake table during the tests; residual wall displacements measured after the tests were negligible.

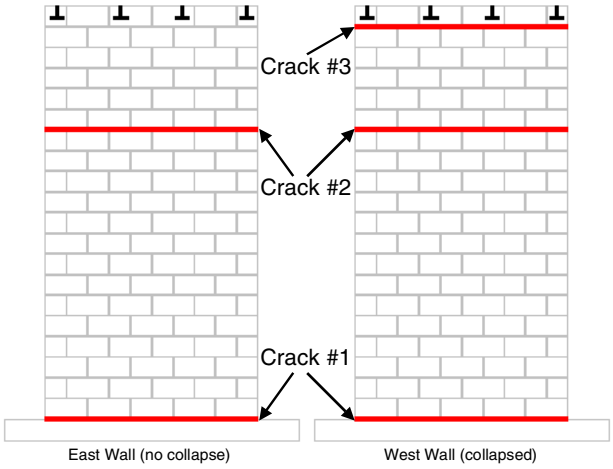

Figure 5a. Final crack pattern on the out-of-plane walls (Run 22).

Figure 5b. Collapse of the West out-of-plane wall (Run 22).

FEMA 306 [6] relates visible damage due to out-of-plane flexural response of URM walls to FEMA 356 [8] performance levels. According to this relation, the slight damage observed in the test specimen would correspond to an Immediate Occupancy performance level, even though such large story drifts would imply Life Safety or Collapse Prevention demand levels. The slight damage at high drift levels may be attributed to the fact that the walls were lightweight with small inertial loading, and the diaphragm was well anchored into the walls through almost perfect pin connections.

During the 22nd test run, the East out-of-plane wall cracked at the bedjoint above the fourteenth course corresponding to 70% of the wall height from the base. This full-length crack is marked as #2 in Figure 5a. Lateral offset or spalling of mortar was not evident at the crack. The wall did not collapse. After the test, the upper 30% portion of the wall was removed. The bedjoint crack #2 was observed to have formed either at top or bottom of the mortar indicating that its formation was due to the loss of masonry bond between the mortar and the block. During the 22nd test run, the West out-of-plane wall with the augmented mass collapsed due to the formation of two full-length horizontal cracks in addition to the already cracked

wall base. The two cracks formed at the bedjoints above the fourteenth course (crack #2) and below the top course (crack #3); their locations are shown in Figure 5a. Video recording showed that the upper and lower portions of the wall between cracks were both in one piece during collapse, behaving like two rigid bodies on top of each other rocking about the cracks. Video also showed that the crack #2 developed just prior to crack #3. It is likely that the shear studs grouted into the top course of the wall forced crack #3 to form below the top course that would otherwise have formed above the top course. A snapshot from the video shows the wall during collapse in Figure 5b.

During the 22nd run, the mid-height displacements of the two walls became out of phase with the wall top displacements. This is demonstrated in Figures 6a and 6b for the East and West Walls, respectively. The East Wall mid-height displacement was in phase with and nearly one-half of the top displacement up to 5.94 seconds into the test run. In Figure 6a, this is observed as the linearly distributed set of data points in the top versus mid-height displacement plot. After 5.94 seconds, however, data points showed closed loop patterns with large deviations from the linear trend. Four points in time were identified as points A, B, C, and D shown in both plots of Figure 6a. Response history for the West Wall in Figure 6b shows the start of out-of-phase response marked by point A at 5.25 seconds into the run. This was followed by points B, C, D, and E marking various instants in time when either the wall top or mid-height displacement peaked. The wall could be considered collapsed after point E when the mid-height displacement (and later the top displacement) became large enough to exceed the range of the displacement transducer. The locations of the five points are also provided in the top versus mid-height displacement plot of Figure 6b that includes data from only the initial 6.00 seconds of the recorded response. The plot shows the linear trend of in phase response followed by an open loop pattern that indicates collapse. Comparison of the occurrence times revealed that the out-of-phase response in the West Wall was initiated earlier than in the East Wall, indicating that the West Wall had cracked and failed just before the East Wall cracked.

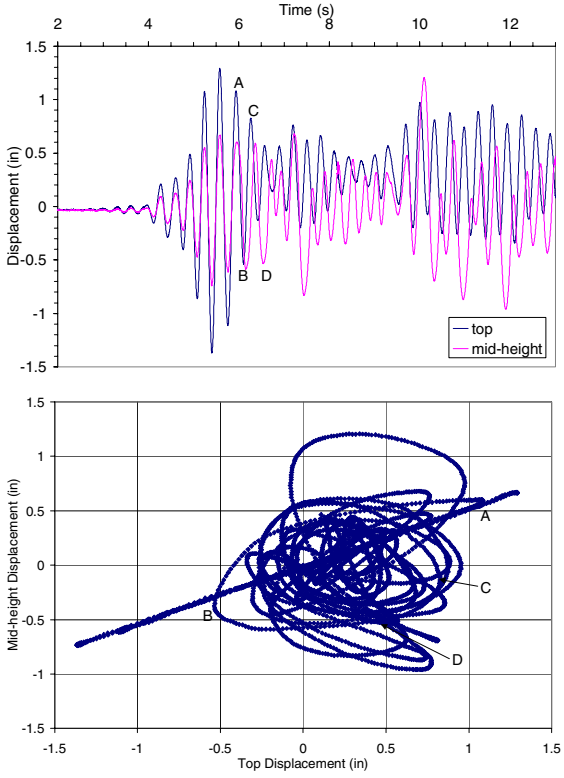

Figure 6a. Comparison of East Wall top and mid-height displacements in Run 22.

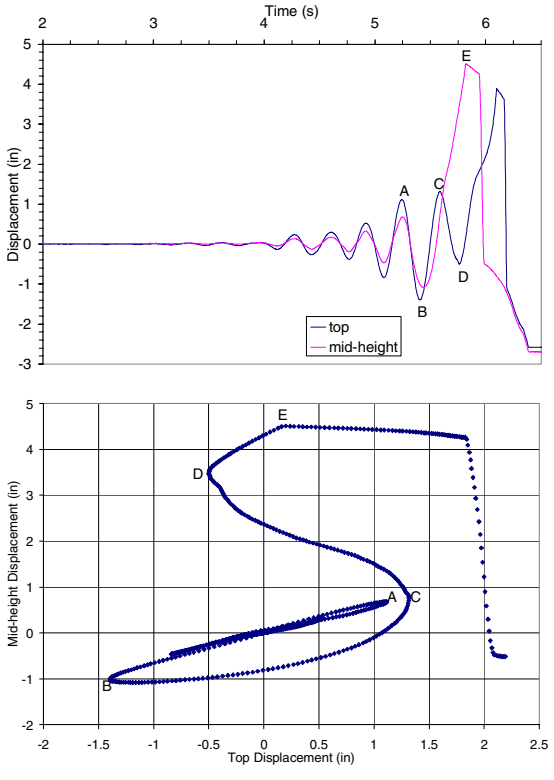

Figure 6b. Comparison of West Wall top and mid-height displacements in Run 22.

Significantly larger out-of-plane wall displacements were measured with specimen S2 than with S1 for test runs with the same ground motion intensity (Table 4). This was attributable to the difference in spectral displacements associated with the frequencies of vibration of specimens with the flexible and stiff diaphragm. Simsir et al. [14] provides more information on the effect of diaphragm flexibility on the out-of-plane wall response.

The measured peak acceleration values were similar at the top and mid-height of the out-of-plane walls for each run (Table 4), and these values were up to 4.5 times the peak base accelerations.

Peak base shear force in the out-of-plane direction was plotted against peak drift for all runs for the East and West Walls as shown in Figures 7a and 7b, respectively. Peak base shear was calculated as the maximum of the sum of the products of the tributary masses and respective accelerations at the wall top, mid-height, and base. Tributary masses consisted of one-half wall mass lumped at the wall mid-height, and one-fourth wall masses lumped at the top and bottom of the wall. Apparent in both Figures 7a and 7b is the direct influence of diaphragm mechanical properties on the behavior of out-of-plane walls. Data points in the two figures are clustered into two trends, one for S1 with stiff diaphragm and the other for S2 with flexible diaphragm. The bilinear nature of the latter trend was due to the yielding of the diaphragm and not due to softening in the wall. Data point for Run 9 looks out of place because of higher than expected accelerations encountered in that run due to loosening and banging of the bolted connection between the diaphragm beam and the in-plane wall. The base shear for Run 21 in West Wall was large compared to that in East Wall due to large inertia caused by the extra mass on West Wall. Base shear for Run 22 in East Wall was larger than expected for the flexible diaphragm trend due to smaller floor mass that resulted in a larger frequency of vibration and larger pseudo-acceleration response (Figure 4).

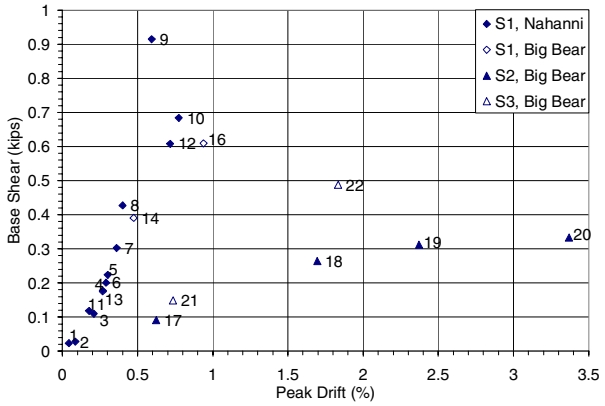

Figure 7a. East Wall peak drift versus peak base shear from Runs 1-22.

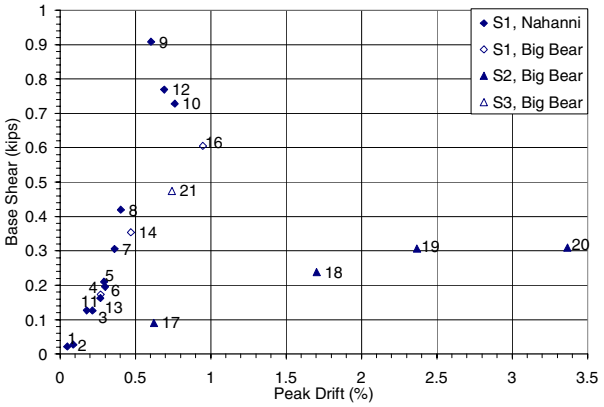

Figure 7b. West Wall peak drift versus peak base shear from Runs 1-21.

Strains in the flexible steel diaphragm beam exceeded yield at mid-span during the 20th run. Strains in the stiff diaphragm beam did not exceed the yield strain through the entire series of tests. One of the in-plane walls sustained diagonal shear cracks during the 15th run. Strain gauge readings indicated that the extreme end longitudinal steel reinforcing bars at the base of the wall exceeded the yield strain during this run. Bars did not yield in the other in-plane wall, which sustained less severe cracking that was concentrated mostly around the base of the wall. With respect to the top of the in-plane walls, diaphragm mid-span response was amplified more during test runs with the flexible diaphragm of S2 and S3 than with the stiff diaphragm of S1. Compared to runs with S1, displacement and acceleration peak amplifications over the duration of the run increased by a factor of approximately 7 and 2 (respectively) during runs with S2.

ANALYTICAL MODELS

Single-Degree-of-Freedom (SDOF) Model

Response of the structure during the first 20 runs can be computed using an SDOF model. The model accounts for the flexibility of the diaphragm and assumes the out-of-plane wall is both strong and rigid as it freely rotates about its base. The spring in Figure 8a represents the stiffnesses of the diaphragm and the in-plane wall connected in series. The diaphragm mass and one-third of the wall mass are lumped at the end of the spring. The one-third ratio was determined by a virtual work analysis of the generalized SDOF system with the assumed deformation configuration shown in Figure 8a. The wall is idealized as a rigid body, rocking about its base, even at small excitation amplitudes. Response was computed using the program USEE (Inel et al. [10]). A linear elastic model was used for the stiff specimen because the diaphragm remained elastic. A bilinear model was used for the flexible specimen, because the diaphragm beam yielded in some runs. Measured values of mass, stiffness, strength, and damping were used directly to determine the properties of the SDOF system. Computed peak displacements from this analysis are compared with the measured values in Figure 8b for the first 20 runs. Displacement and acceleration response histories for these runs can also be computed using USEE. As an example, measured and computed displacement response histories at the top of the wall for the 7th test run are plotted in Figure 9.

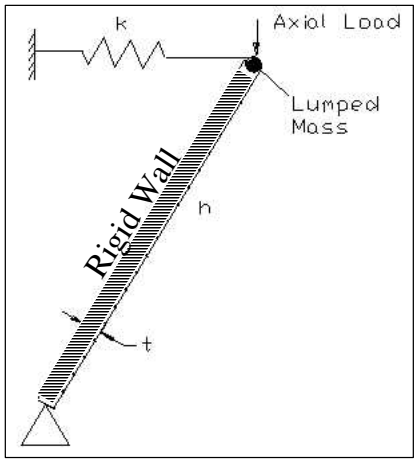

Figure 8a. SDOF model.

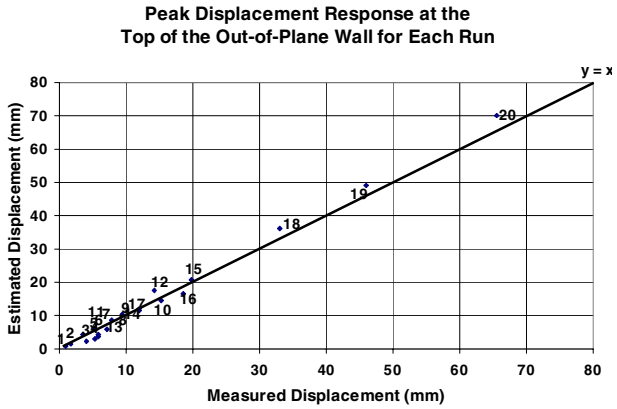

Figure 8b. Correlation between measured and computed response with SDOF model.

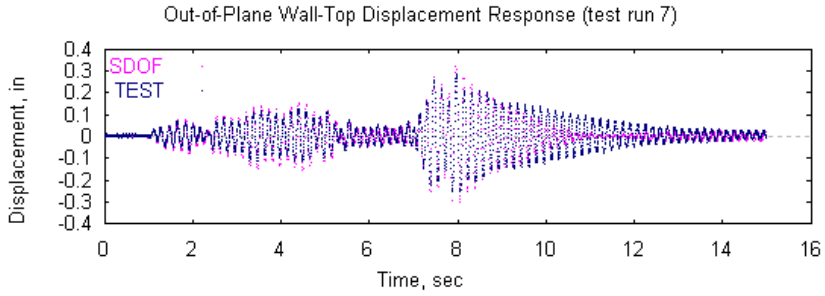

Figure 9. Comparison of measured and computed SDOF response histories.

The SDOF model is inaccurate in the sense that it can not model cracking of the out-of-plane walls such as the formation of crack #2 in Figure 5a. Such cracking is dictated by higher modes that come into play due to the mass distribution of the walls and the diaphragm mass at the top of the wall. The SDOF model can not capture the higher mode response observed in the 22nd test run.

Multi-Degree-of-Freedom (MDOF) Model

To compute the response of an out-of-plane wall that cracks at the bedjoints, an MDOF model was created. The model accounts for the flexibility of the diaphragm, the stiffness of the wall, and the possibility for horizontal cracks developing under combined flexural moments and axial forces. The two springs connected in series in Figure 10 represent the stiffnesses of the in-plane wall and the diaphragm. They both have bilinear behavior with inelastic unloading. Half of the in-plane wall mass is lumped between the two springs, and the diaphragm mass is lumped at the end of the diaphragm spring or at the top node of the out-of-plane wall. The out-of-plane wall is modeled in elevation as a series of concrete blocks and mortar joints. Each concrete block represents all the blocks in one course of the masonry wall. The mass of each course of the wall is lumped at the top and bottom of that course. The block is modeled as a linear elastic beam-column element that ignores shear deformations and is rigid at the interface with the mortar joint. The mortar joint is modeled using a multiple fiber beam-column element that has nonlinear behavior in compression with measured stress-strain values from compression test of mortar. Shear deformations in the mortar joint are not modeled. Using nine fibers in this element resulted in a better representation of measured response than an earlier mortar joint model that had two compression/tension link elements for axial and flexural behavior and an elastic panel element to represent shear in the mortar.

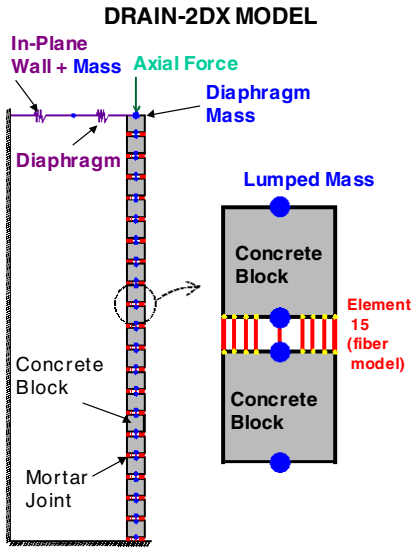

Figure 10. MDOF model.

Response was computed using the program DRAIN-2DX (Prakash et al. [13]) that uses a time-step integration technique for nonlinear dynamic analysis. Second-order (P-Delta) effects were modeled. For the 7th test run (same run of Figure 9), the displacement history at the top of the out-of-plane wall computed using the MDOF model is compared with the measured history in Figure 11.

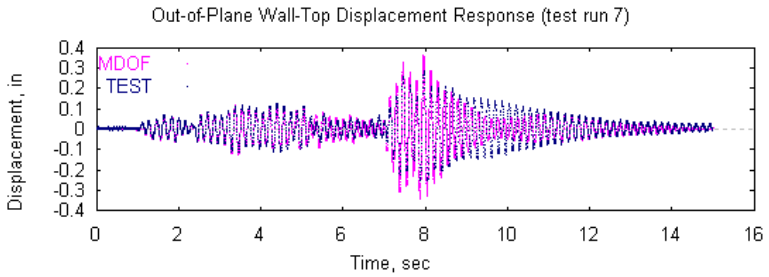

Figure 11. Comparison of measured and computed MDOF response histories.

Two-Degree-of-Freedom (2DOF) Model for Dynamic Stability Analysis

Current seismic guideline FEMA 356 [8] permits flexural cracking in URM out-of-plane walls for Life Safety and Collapse Prevention performance levels provided that the cracked wall segments remain stable during dynamic excitation. FEMA 356 [8] allows slenderness (h/t) ratios larger than those in Table 2 to be used if justified by a dynamic stability analysis, but methods for conducting such an analysis are not specified and thus are largely subject to the discretion of the user. Current research is focused on providing a dynamic analysis tool to determine the stability of URM out-of-plane walls. While such an analysis is possible with the MDOF model presented in this paper, the complexity of the model and the time it takes (5 to 10 minutes depending on the duration of the excitation) to perform the analysis prompted the development of a simpler 2DOF model that is more suitable for professional practice.

The 2DOF model, shown in Figure 12, is an assemblage of two rigid bars interconnected by hinges; relative rotations of the bars are resisted by rotational springs k_1 and k_2 located at the hinges. The two rigid bars represent the cracked wall segments of Figure 5a, with the upper segment having one-third of the wall length and weight. The total length and weight of the wall are denoted by L and W, respectively. W_d is the weight of the floor lumped at the top of the wall. The translational spring k_3 represents the stiffnesses of the in-plane wall and the diaphragm connected in series. The displacement of k_3 is a function of the rotation angles q_1 and q_2 of the rigid bars, as shown in Figure 12. The values for k_1 and k_2 can be determined from the post-cracked static moment-rotation relationships of the wall segments, in which gravity restoring moments oppose overturning moments. This relationship is illustrated in Figure 13 for an idealized rigid case as well as for a real semi-rigid case as put forth by Doherty [5]. The semi-rigid relationship deviates from the rigid bilinear relationship due to the forcing of the vertical reactions towards the extreme compressive faces of the wall.

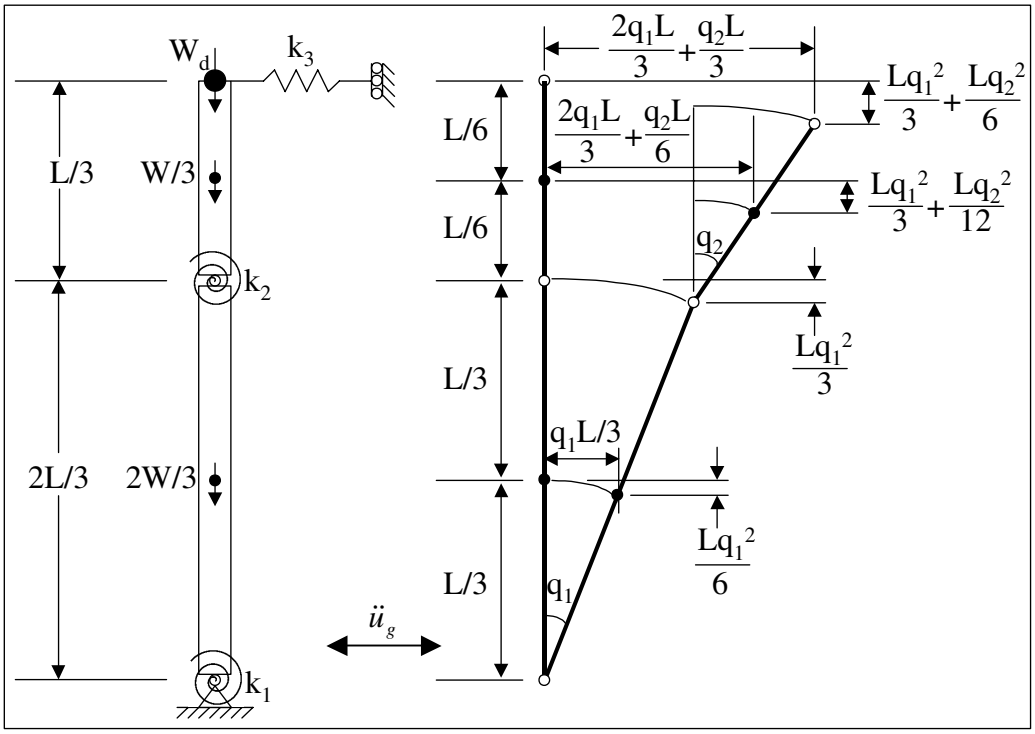

Figure 12. 2DOF model.

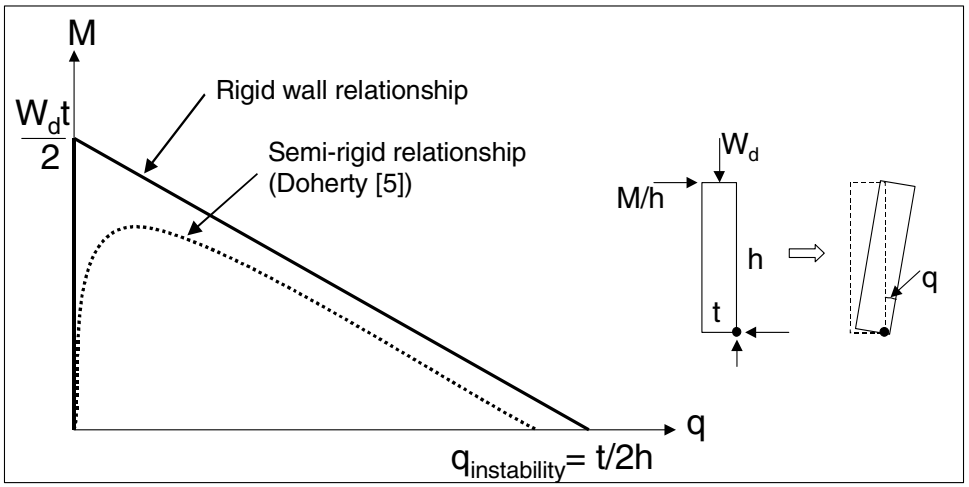

Figure 13. Moment-rotation relationship of a cracked wall segment.

The generalized coordinates of the 2DOF system are taken to be the independent rotation angles q_i of the rigid bars (Figure 12). Equations of motion are formulated from Lagrange's equation by determining the kinetic energy (inertial terms), potential energy (elastic terms), and the non-conservative virtual work (external excitation and internal damping) in the system (Clough and Penzien [4]). Displacements are assumed small, which is acceptable for a wall with a drift ratio less than 3.4% that corresponds to a wall rotation of 1.9°. The total kinetic energy includes the rotation of the rigid bar masses about their individual centroids, and the translation of the centroids and the diaphragm mass (W_d/g - where g is the acceleration of gravity). The total potential energy includes the deformation of the springs k_1, k_2, and k_3, and the lowering of the centers of gravity of the rigid bars and W_d below their vertical base position. Assuming there is no damping in the system, the equations of motion for the two degrees of freedom of the system (in matrix form) are

$$\frac{L^2}{9g}\begin{bmatrix} \frac{80}{9}W + 4W_d & 2(W+W_d) \\ 2(W+W_d) & \frac{19}{36}W + W_d \end{bmatrix}\begin{bmatrix} \ddot{q}_1 \\ \ddot{q}_2 \end{bmatrix}$$

$$+\begin{bmatrix} \frac{1}{9}(-4WL - 6W_d L + 4k_3 L^2) + k_1 + k_2 & \frac{2}{9}k_3 L^2 - k_2 \\ \frac{2}{9}k_3 L^2 - k_2 & \frac{1}{9}(-\frac{1}{2}WL - 3W_d L + k_3 L^2) + k_2 \end{bmatrix}\begin{bmatrix} q_1 \\ q_2 \end{bmatrix} = \begin{bmatrix} p_{eff,1}(t) \\ p_{eff,2}(t) \end{bmatrix}$$

where $\ddot{q}_1$ and $\ddot{q}_2$ are rotational accelerations, the second derivatives of q_1 and q_2 (respectively) with respect to time, and $p_{eff,1}(t)$, $p_{eff,2}(t)$ are the generalized effective force functions generated by the earthquake excitation $\ddot{u}_g$.

Based on the foregoing, a user-friendly visual interface for performing dynamic stability simulations with the 2DOF model is being developed.

CONCLUSIONS

Unreinforced masonry walls were subjected to dynamic actions orthogonal to their plane resulting from simulated earthquake motions on a shake table. Motions resulting from vibration of both stiff and flexible

floor diaphragms were observed in the experimental study and corroborated with results from analog computational models. The following conclusions were drawn from this study.

1. Unlike observed with static testing of out-of-plane walls done by others, no mid-height collapses resulted, except when the axial load was reduced and adding supplemental mass significantly increased wall mass. Rocking at the base of the wall did not cause collapse.

2. Only minor cracks at the base of the wall were apparent through peak drifts as large as 3.4%. The cracks were associated with rocking of the walls at their bases. Residual drifts were negligible (0.13%), and noticeable lateral offsets at the cracks did not occur. The observed damage corresponded to a performance limit state in the range of Immediate Occupancy. To reach Life Safety and Collapse Prevention performance levels, more substantial damage such as spalling of mortar and offsets at the cracks would have had to occur. Such damage was not observed in the present tests.

3. The measured peak acceleration values were similar at the top and mid-height of the out-of-plane walls, and these values were up to 4.5 times the peak base accelerations.

4. As illustrated by the measured relationship of peak base shear versus peak drift in the out-of-plane direction, the influence of diaphragm properties (mass or axial load, stiffness before and after yield) as well as the influence of wall mass on the wall's out-of-plane demand could be detected. The intensity of axial load on the wall and the mass of the wall affected the out-of-plane response. Collapse occurred for reduced axial load and augmented wall mass.

5. Diaphragm flexibility significantly increased the out-of-plane displacement response. This was consistent with the increase in spectral displacement associated with the increase in period that resulted from the flexibility of the diaphragm. Diaphragm flexibility also significantly amplified the diaphragm mid-span displacement and acceleration responses with respect to those of the in-plane walls.

6. Displacement response was computed with reasonable accuracy using a simple SDOF system subjected to the measured table excitations.

7. The MDOF model was helpful in estimating the response as well as detecting bedjoint cracks along the height of the wall. Simulations performed with the model can be used for establishing the allowable wall slenderness ratio.

8. With only two equations of motion, the 2DOF model has the potential use as a simple tool for URM wall stability analysis as prescribed by FEMA 356 [8].

9. Based on observed out-of-plane wall failures in past earthquakes, adequate anchorage of URM walls to the diaphragm is critical to preventing out-of-plane failure.

Tests were performed on a specimen having capable connections that prevented sliding or pullout of the diaphragm relative to the masonry walls. The URM out-of-plane walls were discrete, free-standing elements; that is, not built integrally with the orthogonal reinforced masonry in-plane walls. Thus, the performance of walls subjected simultaneously to out of plane and in plane excitations was not assessed in the present tests. If in plane shear demands are large enough to cause cracking in plane, one may expect more severe out of plane damage than was observed in the present tests.

ACKNOWLEDGMENTS

This work was supported primarily by the Earthquake Engineering Research Centers Program of the National Science Foundation through the Mid-America Earthquake Center under Award Number EEC-9701785. The half-scale concrete hollow blocks used in the experimental setup were provided by the Construction Engineering Research Laboratory (CERL) of the Engineer Research and Development Center, U.S. Army Corps of Engineers.

REFERENCES

1. ABK. "Methodology for Mitigation of Seismic Hazards in Existing Unreinforced Masonry Buildings: Wall Testing, Out-of-Plane, Topical Report 04". ABK Joint Venture, El Segundo, California, December 1981.
2. ABK. "Methodology for Mitigation of Seismic Hazards in Existing Unreinforced Masonry Buildings: The Methodology, Topical Report 08". ABK Joint Venture, El Segundo, CA, 1984.
3. Adham SA. "Static and Dynamic Out of Plane Response of Brick Masonry Walls". Proceedings of the 7th International Brick Masonry Conference, Melbourne, Australia, 1985: 1218-1224.
4. Clough RW, Penzien J. "Dynamics of Structures, 2nd Edition". McGraw-Hill, Inc, 1993: 341-361.
5. Doherty KT. "An Investigation of the Weak Links in the Seismic Load Path of Unreinforced Masonry Buildings". Ph.D. Thesis, The University of Adelaide, Australia, 2000: 73-78.
6. FEMA 306. "Evaluation of Earthquake Damaged Concrete and Masonry Wall Buildings, Basic Procedures Manual". Federal Emergency Management Agency, Washington, D.C., 1999: 180-181.
7. FEMA 307. "Evaluation of Earthquake Damaged Concrete and Masonry Wall Buildings, Technical Resources". Federal Emergency Management Agency, Washington, D.C., May 1999: 78-79.
8. FEMA 356. "Prestandard and Commentary for the Seismic Rehabilitation of Buildings, Report No. FEMA 356". Federal Emergency Management Agency, Washington, D.C., November 2000: 7-18.
9. French S, Olshansky R. "Inventory of Essential Facilities in Mid-America, CD Release 01-01". Mid-America Earthquake Center, Urbana, Illinois, 2001.
10. Inel M, Bretz E, Black EF, Aschheim MA, Abrams DP. "USEE 2001-Utility Software for Earthquake Engineering, Program, Report and User's Manual, CD Release 01-05". Mid-America Earthquake Center, Urbana, Illinois, 2001.
11. Kariotis JC, Ewing RD, Johnson AW, Adham SA. "Methodology for Mitigation of Earthquake Hazards in Unreinforced Brick Masonry Buildings". Proceedings of the 7th International Brick Masonry Conference, Melbourne, Australia, 1985: 1339-1350.
12. Peralta DF, Bracci JM, Hueste MBD. "Project ST-8: Seismic Performance of Rehabilitated Floor and Roof Diaphragms". Presentation, Research Assistant Symposium of the Mid-America Earthquake Center, New Orleans, November 2000.
13. Prakash V, Powell GH, Campbell S. "DRAIN-2DX: Base Program Description and User Guide, Version 1.10". University of California at Berkeley, 1993.
14. Simsir CC, Aschheim MA, Abrams DP. "Response of Unreinforced Masonry Bearing Walls Situated Normal to the Direction of Seismic Input Motions". Proceedings of the 7th US National Conference on Earthquake Engineering, Boston, MA. EERI, July 2002.
15. Simsir CC, Aschheim MA, Abrams DP. "Influence of Diaphragm Flexibility on the Out-of-Plane Response of Unreinforced Masonry Bearing Walls". Proceedings of the 9th North American Masonry Conference, Clemson, SC. The Masonry Society, June 2003.
16. Wen YK, Liao KW. "Modeling Fragility of Essential Facility Structures". Proceedings of the KEERC-MAE Joint Seminar on Risk Mitigation for Regions of Moderate Seismicity, Urbana, IL. Mid-America Earthquake Center, August 2001.